SCIENCE CHINA
Information Sciences

• **RESEARCH PAPER** •

October 2016, Vol. 59 102314:1–102314:16
doi: 10.1007/s11432-015-0503-x

Cognitive frequency diverse array radar with symmetric non-uniform frequency offset

Abdul BASIT[1*], Ijaz Mansoor QURESHI[2], Wasim KHAN[1] & Aqdas Naveed MALIK[1]

[1]*Department of Electronic Engineering, International Islamic University, Islamabad* 44000*, Pakistan;*
[2]*Department of Electrical Engineering, Air University Islamabad, Islamabad* 44000*, Pakistan*

Received December 10, 2015; accepted February 29, 2016; published online August 26, 2016

Abstract Frequency diverse array (FDA) radar with uniform inter-element frequency offset generates a beam pattern with maxima at multiple range and angle values. Multiple maxima property allows interferers located at any of the maxima to affect the target-returns. As a result the signal to interference noise ratio (SINR) and probability of detection decreases. In this paper, we propose a cognitive uniformly-spaced FDA with non-uniform but symmetric frequency offsets to achieve a single maximum beam pattern at the target position. Moreover, these non-uniform frequency offsets are calculated using well known mu-law formulae. The design sharpens or broadens the transmitted beam pattern based on the receiver feedback to achieve a better detection probability and an improved SINR as compared to the previous designs. The performance is also analyzed by considering the Cramer-Rao lower bound (CRLB) on target angle and range estimation.

Keywords cognitive radar, frequency diverse array, non-uniform frequency offset, range-angle beam forming

Citation Basit A, Qureshi I M, Khan W, et al. Cognitive frequency diverse array radar with symmetric non-uniform frequency offset. Sci China Inf Sci, 2016, 59(10): 102314, doi: 10.1007/s11432-015-0503-x

1 Introduction

A flexible beam scanning array named frequency diverse array (FDA) was originally proposed in [1], to provide additional degrees of freedom for adaptive radar applications. It uses a small frequency offset between the adjacent elements of a uniform linear antenna array to generate a 3-D beam pattern as a function of frequency offset, time, range and angle [2]. The beam scanning feature of a conventional FDA, i.e., FDA with a uniform inter-element frequency offset was investigated in [3]. Furthermore, the periodicity of beam pattern in time, range and angle was explored in [4]. Likewise, the range-angle dependent beam forming ability to suppress interferers at different ranges and directions, resulting in improved SINR, was examined in [5]. The small frequency offset plays a vital role to improve the overall performance of an FDA radar, such as controlling the range-angle dependency and spatial distribution of generated beam pattern [6–8]. Therefore, researchers have shown their keen interest to investigate an open question that how to select a proper frequency offset and its application between the adjacent elements of a linear FDA for improved performance. Consequently, an FDA with an adaptive frequency offset selection scheme was proposed in [9] to maximize the output SINR criteria. Likewise, an FDA

* Corresponding author (email: abdulbasit@iiu.edu.pk)

with a time dependent frequency offset was proposed in [10] to achieve an improved time dependent beam pattern for a given target range and direction. Subsequently, the inter-element spacing of FDA proportional to the wavelength for improved range-angle localization of targets, was studied in [11]. In [12], a uniform linear array with logarithmically increasing inter-element frequency offset was presented, which generated a single-maximum beam pattern for an arbitrary value of frequency offset and also suppressed interferences. A simulation based study of an FDA with non-uniform frequency offsets was carried out in [13] to indicate the modified shape of beam pattern in terms of null depths.

The objective of this research is to utilize the basic properties of cognitive radar (CR) [14–17] for improved SINR and detection probability of an FDA with non-uniform frequency offsets applied along the array. Three cognitive radar properties are i) learning through continuous interaction with the environment using intelligent signal processing techniques, ii) using feedback from receiver to the transmitter for optimizing the performance, and iii) preserving the previously collected information [14].

In this paper, a cognitive uniformly-spaced FDA with symmetric non- uniform frequency offsets is proposed to achieve a single maximum beam pattern at the target position based on the feedback, adaptively. The linear FDA block of receiver estimates the direction of arrival (DOA) using multiple signal classification (MUSIC) algorithm [18]. It also calculates the target range using a conventional range estimator. The estimated range and direction of the target are given to the extended Kalman filter (EKF) [19] based prediction block, one of the best choices in hand for nonlinear radar environments, to estimate the target future direction. Based on the accuracy of the predictor block, there can be two cases, i) the estimate is accurate or with affordable error, ii) the estimate is not accurate or the predicted target position is out of range (target is lost). If the position of the target is accurately predicted, the transmitter needs to direct its sharp beam pattern peak, regardless of generated high side lobes, to detect the target. On the contrary, if the target range and angle values are not in the given range or the estimated prediction error is not affordable, the transmitter is set to increase the beam width of the main lobe towards the target previous position to detect the target in the next cycle. Therefore, this prediction error information along with the predicted target position is sent as feedback to the transmitter.

The selector, a sub-block of transmitter, calculates the non-uniform frequency offsets using well known mu-law or μ-law [20–22] in each step. Different values of μ produce a non-uniform expanded or compressed set of the frequency offset across the array, which enables the FDA to generate a single maxima beam pattern for interference suppression along with sharpening or broadening of the main beam. The width of main beam is kept inversely proportional to the prediction accuracy for improved performance. These non-uniform frequency offset values are calculated at each cycle to achieve a better detection probability, an improved SINR and improved CRLB as compared to the previous designs. The symmetric pattern [23] of offsets around the central element achieves better null depths as compared to non-symmetric pattern. The effectiveness of proposed scheme has been evaluated in simulations, which indicates an outclass performance as compared to the previous works.

The rest of the paper is organized as follows: Section 2 analyzes the proposed system, mathematically. Section 3 is reserved for simulations, results and discussions. Finally, Section 4 concludes the paper.

2 Proposed system design

This section describes the block diagram of proposed system design. The proposed receiver consists of four sub-blocks, i.e., DOA and range estimation, receiver selector, EKF-based predictor and memory block. The proposed transmitter consists of two sub-blocks, i.e., transmit selector and FDA antenna block with non-uniform frequency offsets. Figure 1 shows the information flow of proposed system at any time l.

The FDA antenna block of transmitter illuminates the radar environment having potential targets. The DOA and range estimation block of receiver, collect the reflected echoes to estimate the target and interferer DOAs and range using well known MUSIC algorithm and conventional range estimation formula, respectively. The receiver selector, a sub-block of receiver, calculates the weight vector ($\boldsymbol{w}_R$)

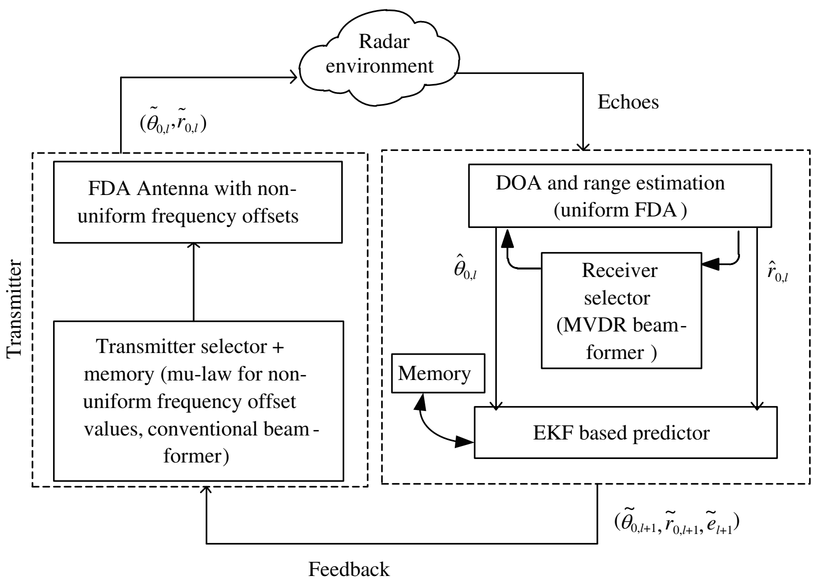

Figure 1 Block diagram of the proposed radar.

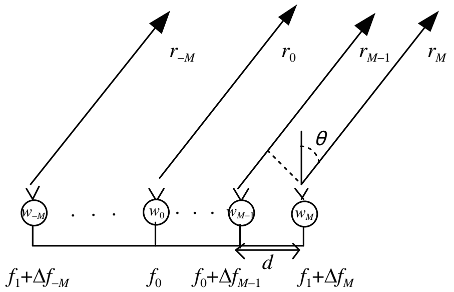

Figure 2 Proposed frequency diverse array transmitter.

using minimum variance distortion less response (MVDR) adaptive beam-former to improve the SINR performance. Consequently, the current target position estimates $(\hat{\theta}_{0,l}, \hat{r}_{0,l})$ are forwarded to the EKF based predictor for estimating the target next position $(\tilde{\theta}_{0,l+1}\,,\, \tilde{r}_{0,l+1})$. This estimated next position and the prediction error $\tilde{e}$ are sent as feedback to the transmitter. The transmit selector, a sub-block of transmitter, decides an appropriate value of μ with the help of a feed forward neural network (NN) based on $\tilde{e}$. It facilitates to calculate non-uniform frequency offset values using mu-law. A conventional beam-former calculates vector $\boldsymbol{w}_T$ to generate maxima in the target predicted direction. The perception-action cycle keeps on repeating itself for improved performance. The transmitter and receiver of the proposed design are discussed below in detail.

2.1 Transmitter

The non-uniform FDA design, calculation of non-uniform frequency offsets and non-uniform FDA transmit beamforming have been discussed below.

2.1.1 *Non-uniform FDA antenna*

Figure 2 shows the proposed uniformly-spaced FDA antenna, having symmetrical elements around the origin. This symmetry is with respect to frequency offsets. The inter-element distance is d and total number of elements are $N = 2M + 1$, here M is the maximum number of elements on each side of array from origin, while w_n is the transmitter weights.

The frequency input at nth element is given as

$$f_n = f_0 + \Delta f_n, \quad n = 0, \pm 1, \ldots, \pm M, \tag{1}$$

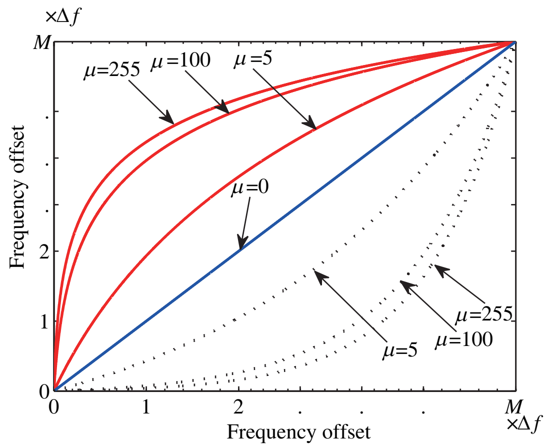

Figure 3 (Color online) Non-uniform frequency offset calculation using mu-law companding schemes.

here, f_0 is the fundamental frequency, Δf_n is the frequency offset of nth element with reference to f_0 and is given as

$$\Delta f_n = \alpha_n \Delta f, \tag{2}$$

here α_n is not an integer, instead it represents a non-uniform coefficient of frequency offset value Δf. The value of middle coefficient is kept zero, i.e., $\alpha_0 = 0$, so that it can transmit waveform with fundamental frequency f_0.

2.1.2 *Calculation of non-uniform frequency offset values using mu-law companding schemes*

Companding schemes [20] are basically composed with a combination of compressing and expanding schemes. These schemes have been used, originally, in communication systems for pulse coded modulation (PCM) transmission to achieve improved signal to quantization error ratio (SQNR) [20], non-linear quantization of pulse coded modulation (PCM) and reducing peak-to-average- power-ratio (PAPR) of orthogonal frequency division multiplexing (OFDM) systems etc [21,22]. In any communication system, the mu-law compression and expansion expression for a given input x can be found as [20]

$$\begin{aligned} F(x) &= \operatorname{sgn}(x) \frac{\ln(1+\mu|x|)}{\ln(1+\mu)}, \quad 0<\mu<255, \\ G(x) &= \frac{1}{\mu}\left(\exp(1+\mu|x|)-1\right)\operatorname{sgn}(x), \quad 0<\mu<255, \end{aligned} \tag{3}$$

where sgn($\cdot$) represents the signum function and value of μ varies form 0–255 in case of 8 bit compression. In our case, we want to calculate the non-uniform frequency offsets for an FDA transmitter by selecting an appropriate companding factor (i.e., suitable values of mu) to achieve an improved performance. The mu-law compression and expansion expression used for calculating non-uniform frequency offsets in this paper, are given as

$$\Delta f_n = \operatorname{sgn}(n\Delta f)\frac{\nu \ln\left(1+\mu\frac{n\Delta f}{\nu}\right)}{\ln(1+\mu)} \text{ and } \Delta f_n = \frac{\nu}{\mu}\left(\exp\left(\frac{\ln(1+\mu)\, n\Delta f}{\nu}\right)-1\right)\operatorname{sgn}(n\Delta f), \quad n=0,\pm1,\ldots,\pm M, \tag{4}$$

where Δf is the input frequency offset, while Δf_n is the calculated frequency offset, μ is a compression factor and ν is a maximum allowable value of Δf. Since, we are assuming a symmetric [23] FDA with $2M+1$ elements, therefore, Figure 3 shows the employed frequency offsets of one side, i.e., M elements. $\mu = 0$ assures no change, solid lines show the compression, while dotted lines show the expansion expression results for different values of μ.

For detailed explanation, Figure 4 shows a comparison of compression and expansion curves with $\mu = 5$.

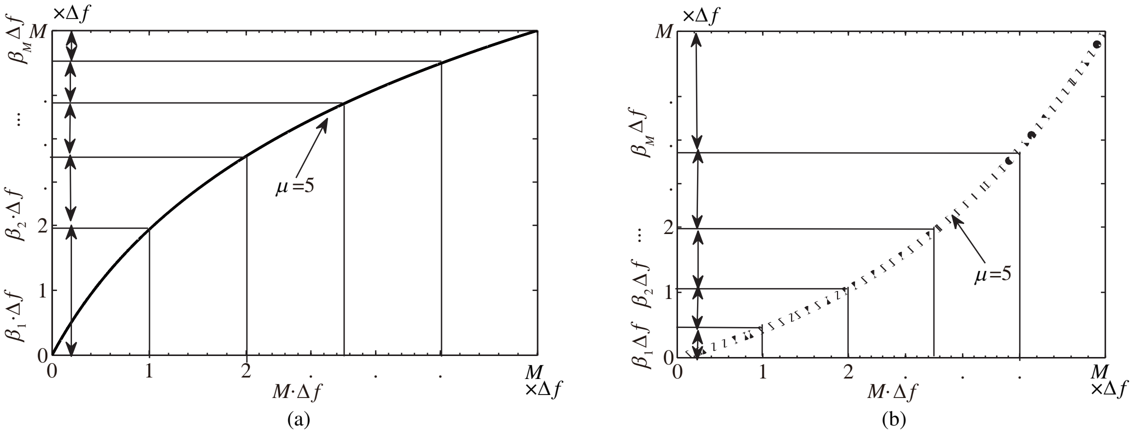

Figure 4 Effect of *mu-law* companding schemes on uniform frequency offsets. (a) Compression; (b) expansion.

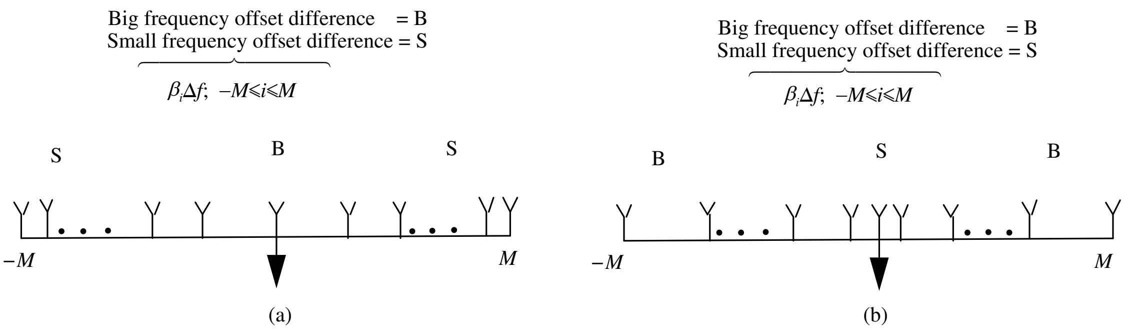

Figure 5 Proposed array structures with respect to the frequency offset difference. (a) SBS array (based on compression scheme); (b) BSB array (based on expansion scheme).

The frequency offset for reference element is zero, i.e., $\Delta f_0 = 0$ and therefore, the frequency offset difference is defined as $\beta_1\Delta f$, which is between first and reference element, i.e.,

$$\Delta f_1 - \Delta f_0 = \beta_1\Delta f = \alpha_1\Delta f. \tag{5}$$

Similarly, the difference for subsequent pairs of adjacent elements, as shown in Figure 4, is

$$\Delta f_2 - \Delta f_1 = \beta_2\Delta f, \tag{6}$$

$$\Delta f_3 - \Delta f_2 = \beta_3\Delta f. \tag{7}$$

Generalizing it for M elements on each side of symmetric array, we have

$$\Delta f_M - \Delta f_{M-1} = \beta_M\Delta f. \tag{8}$$

In the case of mu-law compression scheme, we note that this frequency offset difference is maximum at the first element and decreases as we go away from reference to the last elements. On the contrary, the difference is minimum at the first element, while it keeps on increasing. For a symmetric array [23], two different cases are shown in Figure 5. The SBS (small-big-small) and BSB (big-small-big) offset structures effect the side lobes level (SLL) [24–26] of generated single maximum FDA beam pattern. The BSB offset array structure generates a single maximum FDA broad beam pattern with low SLL, while SBS generates a sharp beam with high SLL. The transmitter array structure along with the companding factor value μ, is selected based on receiver feedback.

The non-uniform coefficients of frequency offset for 1st and 2nd elements are given as

$$\alpha_1 = \beta_1, \tag{9}$$

$$\alpha_2 = \beta_1 + \beta_2. \tag{10}$$

Generalizing it for Mth value

$$\alpha_M = \beta_1 + \beta_2 + \cdots + \beta_M, \tag{11}$$

$$\alpha_M = \alpha_{M-1} + \beta_M. \tag{12}$$

Therefore, a recursive formula for calculating frequency offset for a symmetric array is given as

$$\Delta f_n = (\alpha_{n-1} + \beta_n)\, \Delta f, \quad n = \pm 1, \pm 2, \ldots, \pm M. \tag{13}$$

2.1.3 *Non-uniform FDA beam pattern and transmit beamforming*

Consider a target on θ direction, the phase of signals transmitted by reference and adjacent elements is given by [8]

$$\Psi_0 = \frac{2\pi f_0}{\mathrm{c}} r_0 \quad \text{and} \quad \Psi_1 = \frac{2\pi f_1}{\mathrm{c}} r_1, \tag{14}$$

here, c is speed of light, while r_0 and r_1 are the target distances from reference and adjacent elements, respectively. The frequency $f_1 = f_0 + \Delta f_1$, while $\Delta f_1 = \alpha_1 \Delta f$ and $r_1 = r_0 - d\sin\theta$. The phase difference of these signals is given as

$$\Psi_1 - \Psi_0 = -\frac{2\pi d\sin\theta}{\mathrm{c}}\left[f_0 + \alpha_1\Delta f - \frac{\alpha_1 \Delta f r_0}{d\sin\theta}\right]. \tag{15}$$

Similarly, the phase difference between reference and Mthelement can be written as

$$\Psi_M - \Psi_0 = -\frac{2\pi d\sin\theta}{\mathrm{c}}\left[f_0 M + \alpha_M M\Delta f - \frac{\alpha_M \Delta f r_0}{d\sin\theta}\right], \tag{16}$$

since $f_0 \gg \alpha_M \Delta f$ and $r_0 \gg \alpha_M d\sin(\theta)$, hence the term containing their product, i.e., $\frac{2\pi\alpha_M M\Delta f d\sin\theta}{c}$ may be neglected. In case of far filed targets i.e., $r_n \approx r$, the steering vector $\boldsymbol{u}(\theta, r, \alpha)$ can be taken as

$$\boldsymbol{u}(\theta, r, \alpha) = \begin{bmatrix} \mathrm{e}^{\mathrm{j}\left(\frac{2\pi f_0 M d\sin\theta}{c} - \frac{2\pi\alpha_{-M}\Delta f r}{c}\right)}, \ldots, \mathrm{e}^{\mathrm{j}\left(\frac{2\pi f_0 d\sin\theta}{c} - \frac{2\pi\alpha_{-1}\Delta f r}{c}\right)}, \\ 1,\ \mathrm{e}^{-\left(\mathrm{j}\frac{2\pi f_0 d\sin\theta}{c} - \frac{2\pi\alpha_1\Delta f r}{c}\right)}, \ldots,\ \mathrm{e}^{-\mathrm{j}\left(\frac{2\pi f_0 M d\sin\theta}{c} - \frac{2\pi\alpha_M\Delta f r}{c}\right)} \end{bmatrix}. \tag{17}$$

It can be represented in vector form, given as

$$\boldsymbol{u}(\theta, r) = \boldsymbol{u}(\theta) \odot \boldsymbol{u}(r, \alpha), \tag{18}$$

where

$$\boldsymbol{u}(\theta) = \left[\mathrm{e}^{\mathrm{j}\left(\frac{2\pi f_0 M d\sin\theta}{c}\right)}, \ldots, \mathrm{e}^{\mathrm{j}\left(\frac{2\pi f_0 d\sin\theta}{c}\right)}, 1,\ \mathrm{e}^{-\mathrm{j}\left(\frac{2\pi f_0 d\sin\theta}{c}\right)}, \ldots,\ \mathrm{e}^{-\mathrm{j}\left(\frac{2\pi f_0 M d\sin\theta}{c}\right)}\right], \tag{19}$$

$$\boldsymbol{u}(r, \alpha) = \left[\mathrm{e}^{-\mathrm{j}\left(\frac{2\pi\alpha_{-M}\Delta f r}{c}\right)}, \ldots, \mathrm{e}^{-\mathrm{j}\left(\frac{2\pi\alpha_{-1}\Delta f r}{c}\right)}, 1,\ \mathrm{e}^{\mathrm{j}\left(\frac{2\pi\alpha_1\Delta f r}{c}\right)}, \ldots,\ \mathrm{e}^{\mathrm{j}\left(\frac{2\pi\alpha_M\Delta f r}{c}\right)}\right]. \tag{20}$$

The FDA beam pattern is a function of (θ) and (r), therefore, following observations are in line [8–13]. i) If $\Delta f = 0$, it reduces to a conventional phased array radar (PAR) pattern ii) If α_n values are taken uniform, a conventional FDA beam pattern is generated. If a desired target position is at (θ''), then the weights for steered beam pattern to achieve a maximum gain, are

$$w_{T,n} = \exp\left\{-\mathrm{j}2\pi f_n\left(\frac{\alpha_n \Delta f \hat{r}_0}{\mathrm{c}} - \frac{n d\sin(\hat{\theta}_0)}{\mathrm{c}}\right)\right\},\ n = 0, \pm 1, \ldots, \pm M, \tag{21}$$

where $w_{T,n}$ is a weight of nth transmitter element. The array factor of an FDA system is given by

$$A = \sum_{n=-M}^{M} w_n \exp\left\{-\mathrm{j}\left(\frac{2\pi f_0 n d\sin\theta}{\mathrm{c}} - \frac{2\pi\alpha_n \Delta f r}{\mathrm{c}}\right)\right\}. \tag{22}$$

The pattern towards a desired target can be approximated as the magnitude squared of array factor [12], given by

$$B\left(r_0,\theta_0,\alpha\right)\approx\left|\sum_{n=-M}^{M}\exp\left\{-\mathrm{j}2\pi\left(\frac{f_0nd\sin(\theta-\hat{\theta}_0)}{\mathrm{c}}-\frac{\alpha_n\Delta f(r-\hat{r}_0)}{\mathrm{c}}\right)\right\}\right|^2. \tag{23}$$

The simulations have been carried out and results are shown for non-uniform frequency offsets in the next section.

2.2 Receiver

The DOA and range estimation, EKF based prediction algorithm and performance analysis of proposed system have been discussed below.

2.2.1 *DOA estimation using ROOT MUSIC algorithm*

ROOT MUSIC algorithm, one of the well-known DOA estimation algorithms, has been used to estimate the target direction in this paper. It can resolve multiple signal directions, simultaneously [18]. Consider a conventional symmetric FDA having $P=2K+1$ elements with inter element distance taken as $d=\lambda/2$. Let θ_0 be the direction of the target to be estimated, measured from the middle element, i.e., origin of the array in this case. Considering uniform weights at the receiver array, signal received by mth element is given by

$$x_m\left(t\right)=s_T\left(t-\frac{r_0}{\mathrm{c}}\right)\exp\left\{\mathrm{j}2\pi f_m\left(t-\frac{r_m}{\mathrm{c}}\right)\right\}+n_m(\mathrm{t}),\ \ m=0,\pm1,\ldots,\pm K. \tag{24}$$

And total signal received at the array input is

$$x_m\left(t\right)=s_T\left(t-\frac{r_0}{\mathrm{c}}\right)\sum_{m=-K}^{K}\exp\left\{\mathrm{j}2\pi f_m\left(t-\frac{r_m}{\mathrm{c}}\right)\right\}+n_m(t), \tag{25}$$

where $f_m=f_0+m\Delta f;\ m=0,\pm1,\ldots,\pm K$ and $r_m=r_{\mathrm{ref}}-md\sin\theta_0$.

Defining $\varphi_1=2\pi f_m\left(t-\frac{r_{\mathrm{ref}}}{\mathrm{c}}\right)$ and $\varphi_m=2\pi f_m\left(t-\frac{md\sin\theta_0}{\mathrm{c}}\right)$, the above equation we can rewritten as

$$x_m\left(t\right)=s_T\left(t-\frac{R_0}{\mathrm{c}}\right)\exp\left(\mathrm{j}\varphi_1\right)\sum_{m=-K}^{K}\exp\left(\mathrm{j}\varphi_m\right)+n_m(t). \tag{26}$$

Defining $s_T\left(t-\frac{R_0}{\mathrm{c}}\right)\exp\left(\mathrm{j}\varphi_1\right)=S\left(t\right)$, therefore, representing it in vector form

$$\begin{bmatrix}x_{-K}\left(t\right)\\ \vdots\\ x_K\left(t\right)\end{bmatrix}=S\left(t\right)\begin{bmatrix}\exp\left(\mathrm{j}\varphi_{-K}\right)\\ \vdots\\ \exp\left(\mathrm{j}\varphi_K\right)\end{bmatrix}+\begin{bmatrix}n_{-K}\left(t\right)\\ \vdots\\ n_K\left(t\right)\end{bmatrix}. \tag{27}$$

Or equivalently, it can written as

$$\boldsymbol{x}\left(t\right)=S\left(t\right)\left(\boldsymbol{a}\left(\varphi\right)\right)+\boldsymbol{n}\left(t\right), \tag{28}$$

here $\boldsymbol{a}\left(\varphi\right)$ is the steering vector. We assume that L far field target signals are impinging on the array, then the output of array can be written as (ignoring t without the loss of generality)

$$\boldsymbol{U}=\sum_{l=0}^{L-1}S_l\boldsymbol{a}(\varphi_l)+\boldsymbol{n}. \tag{29}$$

The covariance matrix $\boldsymbol{R}_u$ is given as

$$\boldsymbol{R}_u=\boldsymbol{A}\boldsymbol{R}_s\boldsymbol{A}^{\mathrm{H}}+\sigma_n^2\boldsymbol{I}. \tag{30}$$

If $\lambda_1 \geqslant \lambda_2 \geqslant \lambda_3 \cdots \geqslant \lambda_P$ be the eigen values of this matrix $\boldsymbol{R}_u$, $v_1 \geqslant v_2 \cdots \geqslant v_L$ be the eigen values of $\boldsymbol{A}\boldsymbol{R}_s\boldsymbol{A}^{\mathrm{H}}$ and $\boldsymbol{q}_1, \boldsymbol{q}_2, \boldsymbol{q}_3, \ldots, \boldsymbol{q}_P$ be eigen vectors of $\boldsymbol{R}_u$, then we can state that

$$\lambda_i = \begin{cases} v_i + \sigma_n^2, & i = 1, 2, \ldots, L, \\ \sigma_n^2, & i = L+1, \ldots, P. \end{cases} \tag{31}$$

Therefore, $\boldsymbol{A}^{\mathrm{H}}\boldsymbol{q}_i = 0\,;\; i = L = 1, \ldots, P$ i.e. $a_k^{\mathrm{H}}(\varphi)\,\boldsymbol{q}_i = 0$, $i = L+1, \ldots, P$ and $k = 1, \ldots, L$. The spatial spectrum $P_{\mathrm{mu}}(\varphi)$ generated by root music algorithm has been given as

$$P_{\mathrm{mu}}(\varphi) = \frac{1}{\boldsymbol{a}^{\mathrm{H}}(\varphi)\,\boldsymbol{E}_n\boldsymbol{E}_n^{\mathrm{H}}\boldsymbol{a}(\varphi)}, \tag{32}$$

where $\boldsymbol{E}_n = [\boldsymbol{q}_{L+1}\,\boldsymbol{q}_{L+2}\cdots\boldsymbol{q}_P]$ and $\boldsymbol{a}(\varphi)$is the signal steering vector. After calculation of the spatial spectrum, DOA estimation can be obtained by searching the peaks. Number of snapshots is 200 for this case.

2.2.2 *Target range estimation*

The time delay to reach the target using FDA beam pattern depends upon the distance of target from transceiver and frequency offset value used [4]. Therefore, time t_d taken by a transmitted signal to reach a far field target is [4, 27]

$$t_d = \frac{\hat{r}_0}{\mathrm{c}} + \left[g - \frac{d}{\lambda}\sin\left(\hat{\theta}_0\right)\right]\left(\frac{1}{\Delta f}\right), \tag{33}$$

where c is speed of light, $\hat{r}_0$ is the estimated range of far field target, $\hat{\theta}_0$ is the estimated target direction, Δf is frequency offset and integer g is for grating lobes. The time t_r taken by reflected echo to reach the receiver is

$$t_r = \frac{\hat{r}_0}{\mathrm{c}}. \tag{34}$$

With the estimated angle information $(\hat{\theta}_0)$ and $T_d = t_d + t_r$, the target range can be calculated as [27]

$$\hat{r}_0 = \frac{\mathrm{c}}{2}\left[T_d - \left\{g - \frac{d}{\lambda}\sin\left(\hat{\theta}_0\right)\right\}\left(\frac{1}{\Delta f}\right)\right]. \tag{35}$$

2.2.3 *EKF algorithm for position prediction estimation*

For a radar environment, which is assumed nonlinear but can be made locally linear, EKF is one of the best choices in hand for implementation of prediction block [19]. The process equation is described by [19, 27]

$$\boldsymbol{x}_{l+1} = \tilde{\boldsymbol{F}}\boldsymbol{x}_l + \boldsymbol{n}_l, \tag{36}$$

where $\boldsymbol{x}_l$ denotes the state of system at discrete time l, $\tilde{\boldsymbol{F}}$ denotes a nonlinear transition matrix, while n_l denotes process noise assumed to be zero mean Gaussian noise with covariance matrix $\boldsymbol{Q}$ as

$$\boldsymbol{E}\left[\boldsymbol{n}_l\boldsymbol{n}_n^{\mathrm{T}}\right] = \boldsymbol{Q}_l\delta_{nl}. \tag{37}$$

Likewise, the measurement equation is described as

$$\boldsymbol{z}_l = \tilde{\boldsymbol{H}}\boldsymbol{x}_l + \boldsymbol{v}_l, \tag{38}$$

where $\boldsymbol{z}_l$ denotes an observation vector at discrete time l, $\tilde{\boldsymbol{H}}$ is a nonlinear measurement matrix, while v_l is measurement noise assumed to be zero mean Gaussian with covariance matrix $\boldsymbol{R}$, given as

$$\boldsymbol{E}\left[\boldsymbol{v}_l\boldsymbol{v}_n^{\mathrm{T}}\right] = \boldsymbol{R}_l\delta_{nl}. \tag{39}$$

The Gaussian distribution can be completely characterized by a mean and covariance and so is given as [19,27]

$$\hat{\boldsymbol{x}}_{l/l} = \mathrm{E}\left[\boldsymbol{x}_l|\boldsymbol{z}_1^l\right], \quad \hat{\boldsymbol{x}}_{l+1/l} = \mathrm{E}\left[\boldsymbol{x}_{l+1}|\boldsymbol{z}_1^l\right]. \tag{40a}$$

Similarly, the filtered and predicted covariance matrices are given as [19]

$$\begin{aligned}\hat{\boldsymbol{P}}_{l/l} &= \mathrm{E}\left[\left(\boldsymbol{x}_l - \hat{\boldsymbol{x}}_{l/l}\right)\left(\boldsymbol{x}_l - \hat{\boldsymbol{x}}_{l/l}\right)^{\mathrm{T}}\middle|\boldsymbol{z}_1^l\right],\\ \hat{\boldsymbol{P}}_{l+1/l} &= \mathrm{E}\left[\left(\boldsymbol{x}_{l+1} - \hat{\boldsymbol{x}}_{l+1/l}\right)\left(\boldsymbol{x}_{l+1} - \hat{\boldsymbol{x}}_{l+1/l}\right)^{\mathrm{T}}\middle|\boldsymbol{z}_1^l\right].\end{aligned} \tag{40b}$$

Hence, the state prediction error $\tilde{\boldsymbol{x}}_{l+1/l}$ and prediction measurement error $\tilde{\boldsymbol{e}}$ are defined as

$$\tilde{\boldsymbol{x}}_{l+1/l} \triangleq \boldsymbol{x}_{l+1} - \hat{\boldsymbol{x}}_{l+1/l}, \tag{41}$$

$$\tilde{\boldsymbol{e}}_{l+1/l} \triangleq \mathbf{z}_{l+1} - \hat{\boldsymbol{z}}_{l+1/l}, \tag{42}$$

where $\hat{\boldsymbol{x}}_{l+1/l} = \tilde{\boldsymbol{F}}\hat{\boldsymbol{x}}_{l/l}$ and $\hat{\boldsymbol{z}}_{l+1/l} = \tilde{\boldsymbol{H}}_{l+1}\hat{\boldsymbol{x}}_{l+1/l}$.

The prediction and prediction measurement error should be minimized, which strongly depend on the echoes.

2.2.4 *Transmit/receive beamforming*

The proposed FDA antenna has the ability to direct beam pattern maximum towards the target look angle and range. Let the signal received at target be given as [28]

$$\boldsymbol{w}_T^{\mathrm{H}}\boldsymbol{a}\left(\theta, r, \alpha\right) s(l), \tag{43}$$

where $\boldsymbol{a}\left(\theta, r, \alpha\right)$ is the transmit steering vector, $s\left(l\right)$ is a transmit signal samples at any discrete time interval l and $\boldsymbol{w}_T^{\mathrm{H}}$ is the transmit beamforming weight vector. The target location is estimated as $(\hat{\theta}_0, \hat{r}_0)$ and interference sources estimated locations are at positions $(\hat{\theta}_i, \hat{r}_i)$. Therefore, the signal at uniform FDA receiver is given by [28, 29]

$$y\left(l\right) = \alpha\boldsymbol{b}\left(\hat{\theta}_0, \hat{r}_0, \Delta f\right) s\left(l\right) + \sum_i \beta_i\boldsymbol{b}\left(\hat{\theta}_i, \hat{r}_i, \Delta f\right) s\left(l\right) + n\left(l\right), \tag{44}$$

where $\alpha = \boldsymbol{w}_T^{\mathrm{H}}\boldsymbol{a}(\hat{\theta}_0, \hat{r}_0, \alpha)$, is directional gains towards the target direction and range, while $\beta_i = \boldsymbol{w}_T^{\mathrm{H}}\boldsymbol{a}(\hat{\theta}_i, \hat{r}_i, \alpha)$ is the directional gain in the interference directions $\hat{\theta}_i$ and ranges $\hat{r}_i$, respectively. $\boldsymbol{b}(\hat{\theta}_0, \hat{r}_0, \Delta f)$ is receive steering vector, while $n(l)$ is zero mean additive white Gaussian noise (AWGN) with σ_n^2 variance. Defining $\boldsymbol{u}_i(\hat{\theta}_i, \hat{r}_i, \Delta f) \triangleq \beta_i\boldsymbol{b}(\hat{\theta}_i, \hat{r}_i, \Delta f)$ and $\boldsymbol{u}_0(\hat{\theta}_0, \hat{r}_0, \Delta f) \triangleq \alpha\boldsymbol{b}(\hat{\theta}_0, \hat{r}_0, \Delta f)$, the array output $\boldsymbol{y}$, after match filtering is given by [28]

$$\boldsymbol{y} = \boldsymbol{u}_0(\hat{\theta}_0, \hat{r}_0, \Delta f) + \sum_i \boldsymbol{u}_i(\hat{\theta}_i, \hat{r}_i, \Delta f) + \boldsymbol{n}. \tag{45}$$

The minimum variance distortion less response (MVDR) beam former calculates the receiver weight vector $\boldsymbol{w}_R$ to suppress the interferences, while giving distortion less response in the target direction and range, is given by [28]

$$\boldsymbol{w}_R = \frac{\hat{\boldsymbol{R}}_{i+n}^{-1}\boldsymbol{u}_0\left(\hat{\theta}_0, \hat{r}_0, \Delta f\right)}{\boldsymbol{u}_0\left(\hat{\theta}_0, \hat{r}_0, \Delta f\right)^{\mathrm{H}}\hat{\boldsymbol{R}}_{i+n}^{-1}\boldsymbol{u}_0\left(\hat{\theta}_0, \hat{r}_0, \Delta f\right)}. \tag{46}$$

$\hat{\boldsymbol{R}}_{i+n}$ is interference plus noise covariance matrix and is given as [28]

$$\hat{\boldsymbol{R}}_{i+n} = \sum_i \sigma_i^2\boldsymbol{u}_i\left(\hat{\theta}_i, \hat{r}_i, \Delta f\right)\boldsymbol{u}_i^{\mathrm{H}}\left(\hat{\theta}_i, \hat{r}_i, \Delta f\right) + \sigma_n^2\boldsymbol{I}. \tag{47}$$

It is estimated using 20 snapshots in this case. Here, it is assumed that the target/ interferences complex amplitudes are mutually uncorrelated with zero mean and variance σ_i^2. The SINR is evaluated as [28, 29]

$$\mathrm{SINR} = \frac{\sigma_s^2\left|\boldsymbol{w}_R^{\mathrm{H}}\boldsymbol{u}_0\left(\hat{\theta}_0, \hat{r}_0, \Delta f\right)\right|^2}{\boldsymbol{w}_R^{\mathrm{H}}\hat{\boldsymbol{R}}_{i+n}^{-1}\boldsymbol{w}_R} \tag{48}$$

$$= \frac{\sigma_s^2 N^2 P^2}{\sum_i \sigma_i^2 \left| \boldsymbol{a}^{\mathrm{H}} \left(\hat{\theta}_0, \hat{r}_0, \alpha \right) \boldsymbol{a} \left(\hat{\theta}_i, \hat{r}_i, \alpha \right) \right|^2 \left| \boldsymbol{b}^{\mathrm{H}} \left(\hat{\theta}_0, \hat{r}_0, \Delta f \right) \boldsymbol{b} \left(\hat{\theta}_i, \hat{r}_i, \Delta f \right) \right|^2 + \sigma_n^2 P}, \tag{49}$$

here, σ_s^2 is variance of the desired target. In the background of weak interferences, SINR term reduces to [28, 29]

$$\mathrm{SINR} \simeq \frac{\sigma_s^2 N^2 P}{\sigma_n^2}. \tag{50}$$

But in the background of a strong interference, SINR term can be expressed as [28, 29]

$$\mathrm{SINR} \simeq \frac{\sigma_s^2 N^2 P^2}{\sum_i \sigma_i^2 \left| \boldsymbol{a}^{\mathrm{H}} \left(\hat{\theta}_0, \hat{r}_0, \alpha \right) \boldsymbol{a} \left(\hat{\theta}_i, \hat{r}_i, \alpha \right) \right|^2 \left| \boldsymbol{b}^{\mathrm{H}} \left(\hat{\theta}_0, \hat{r}_0, \Delta f \right) \boldsymbol{b} \left(\hat{\theta}_i, \hat{r}_i, \Delta f \right) \right|^2}. \tag{51}$$

A more focused transmit beam pattern may result in suppressing interferences effectively.

2.2.5 *Probability of detection analysis*

The signal at receiver array after interference suppression, can be given as

$$\boldsymbol{y} = \boldsymbol{w}_T^{\mathrm{H}} \boldsymbol{a} \left(\hat{\theta}_0, \hat{r}_0, \alpha \right) \boldsymbol{b} \left(\hat{\theta}_0, \hat{r}_0, \Delta f \right) + \boldsymbol{n}, \tag{52}$$

where $\boldsymbol{b}(\hat{\theta}_0, \hat{r}_0, \Delta f)$ is the receive steering vector, while $\boldsymbol{w}_T^{\mathrm{H}} \boldsymbol{a}(\hat{\theta}_0, \hat{r}_0, \alpha)$ is complex amplitude of the steered target. $\boldsymbol{n}$ is AWGN with zero mean and variance σ_n^2. The hypothesis testing problem of a radar detection is modeled as [29]

$$\begin{cases} H_0 : \boldsymbol{y} = \boldsymbol{n}, \\ H_1 : \boldsymbol{y} = \boldsymbol{w}_T^{\mathrm{H}} \boldsymbol{a} \left(\hat{\theta}_0, \hat{r}_0, \alpha \right) \boldsymbol{b} \left(\hat{\theta}_0, \hat{r}_0, \Delta f \right) + \boldsymbol{n}. \end{cases} \tag{53}$$

The probability density function (PDF) of H_0 and H_1 are given as [29]

$$p\left(\boldsymbol{y}; H_0\right) = \exp\left(-\frac{\|\boldsymbol{y}\|^2}{\sigma_n^2} \right), \tag{54}$$

$$p\left(\boldsymbol{y}; H_1\right) = \exp\left(-\frac{\|\boldsymbol{y}\|^2}{\sigma_n^2} \right) \times \exp\left(-\frac{|\|\boldsymbol{w}_T^{\mathrm{H}} \boldsymbol{a}(\hat{\theta}_0, \hat{r}_0, \alpha)\|^2 \|\boldsymbol{b}(\hat{\theta}_0, \hat{r}_0, \Delta f)\|^2 + n|^2}{2\sigma_n^2} \right). \tag{55}$$

The likelihood ratio test is given as [29]

$$\wedge = \log \frac{p\left(\boldsymbol{y}; H_1\right)}{p\left(\boldsymbol{y}; H_0\right)} = \left| \left\| \boldsymbol{w}_T^{\mathrm{H}} \boldsymbol{a} \left(\hat{\theta}_0, \hat{r}_0, \alpha \right) \right\|^2 \left\| \boldsymbol{b} \left(\hat{\theta}_0, \hat{r}_0, \Delta f \right) \right\|^2 + n \right|^2 \underset{H_1}{\overset{H_0}{\lessgtr}} \eta, \tag{56}$$

where η is threshold for detection. The Neyman-Pearson probability of detection and false alarm is given as [29]

$$p_{\mathrm{fa}} = p\left(\wedge > \eta | H_0\right) = 1 - F_{\chi^2_{(2)}} \left(\frac{2\eta}{\sigma_n^2} \right), \tag{57}$$

$$p_{\mathrm{d}} = p\left(\wedge > \eta | H_1\right) = 1 - F_{\chi^2_{(2)}} \left(\frac{\sigma_n^2 F^{-1}_{\chi^2_{(2)}} \left(1 - p_{\mathrm{fa}}\right)}{\sigma_s^2 N^2 P^2 + \sigma_n^2} \right), \tag{58}$$

where P and N are the receiving and transmitting array elements, $\chi^2_{(2)}$ is the chi-square distribution with 2 degrees-of-freedom, δ_s^2 is the target signal power, while $F(\cdot)$ is cumulative distribution function.

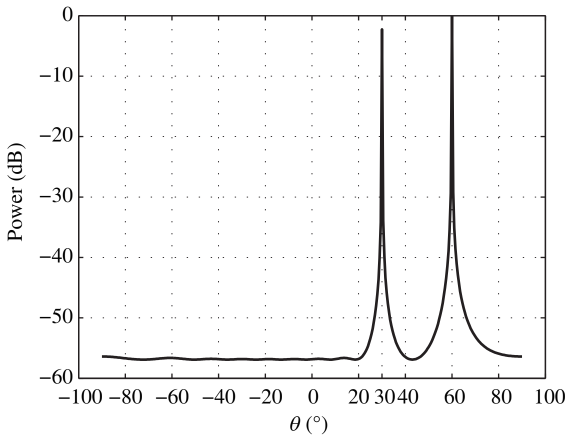

Figure 6 DOA estimation using Root Music algorithm.

2.2.6 *CRLB analysis*

In this section, the performance of proposed scheme has been analyzed in terms of Cramer-Rao Lower Bound (CRLB) criteria for range and angle estimation. For CRLB, the data vector can be taken as [30] $\boldsymbol{y} = (\boldsymbol{w}_T^{\mathrm{H}}\boldsymbol{a}(\hat{\theta}_0, \hat{r}_0, \alpha))\boldsymbol{b}(\hat{\theta}_0, \hat{r}_0, \Delta f) + \boldsymbol{n}$. Therefore, the output in SNR terms is given as $\boldsymbol{y} = \sqrt{\mathrm{SNR}}\,\boldsymbol{b}(\hat{\theta}_0, \hat{r}_0, \Delta f) + \boldsymbol{n}$. Assume that target range-angle vector $\gamma = [\hat{\theta}_0, \hat{r}_0]^{\mathrm{T}}$ is unknown. The Fisher information matrix (FIM) is given as [28]

$$\boldsymbol{J} = 2\mathrm{Re}\left[\frac{d\varepsilon^*}{d\gamma}\boldsymbol{\Gamma}^{-1}\frac{d\varepsilon}{d\gamma^T}\right] = 2\mathrm{SNR}\begin{bmatrix} J_{\hat{\theta}_o\hat{\theta}_o} & J_{\hat{\theta}_o\hat{r}_0} \\ J_{\hat{r}_0\hat{\theta}_o} & J_{\hat{r}_0\hat{r}_0}\end{bmatrix}, \tag{59}$$

where $\varepsilon = \sqrt{\mathrm{SNR}}\,\boldsymbol{b}\left(\hat{\theta}_0, \hat{r}_0, \Delta f\right)$ is mean and $\boldsymbol{\Gamma} = \boldsymbol{I}$ is covariance, while, $J_{\hat{\theta}_o\hat{\theta}_o}$, $J_{\hat{r}_0\hat{r}_0}$ and $J_{\hat{\theta}_o\hat{r}_0}$ values are derived as [30]

$$J_{\hat{\theta}_o\hat{\theta}_o} = \frac{4\pi^2 f_0^2 d^2 \cos^2\left(\hat{\theta}_0\right)}{c^2}\sum_{n=-K}^{K} n^2, \tag{60}$$

$$J_{\hat{r}_0\hat{r}_0} = \frac{4\pi^2 \Delta f^2}{c^2}\sum_{n=-K}^{K} n^2, \tag{61}$$

$$J_{\hat{\theta}_0\hat{r}_0} = J_{\hat{r}_0\hat{\theta}_0} = \frac{4\pi^2 f_0 \Delta f d \cos\left(\hat{\theta}_0\right)}{c^2}\sum_{n=-K}^{K} n^2. \tag{62}$$

The CRLB for the target angle and range estimates can be given as the diagonal elements of the inverse $\boldsymbol{J}$ matrix, i.e., $\mathrm{CRLB}_{\theta_0\theta_0} = [\boldsymbol{J}^{-1}]_{1,1}$ and $\mathrm{CRLB}_{r_0r_0} = [\boldsymbol{J}^{-1}]_{2,2}$.

3 Simulations, results and discussion

This section describes the simulations and results. We assume a symmetric FDA of $N = 11$ transmitting array elements and $P = 11$ receiving array elements with half wave length inter-element distance. The AWGN is modeled as having a zero mean and equal variance at both ends. The carrier frequency $f_0 =$ 10 GHz and $\Delta f = 30$ kHz.

Figure 6 shows the DOA estimation results of Root MUSIC algorithm. The snapshots are 200, while the SNR= 20 dB. Two signals impinge on the receiving array from 30° and 60° simultaneously. 30° is the target direction, while 60° is the direction of interference. The employed algorithm estimates the DOA quite accurately. Likewise, the range of these targets can be easily estimated using the derived range estimation formula. The current estimated range and direction of the target i.e., $(\hat{\theta}_{9,k}, \hat{r}_{0,k})$, along with the previously estimated positions kept in the memory, i.e., $(\hat{\theta}_{0,k-1}, \hat{r}_{0,k-1})(\hat{\theta}_{0,k-2}, \hat{r}_{0,k-2})(\hat{\theta}_{0,k-3}, \hat{r}_{0,k-3})$

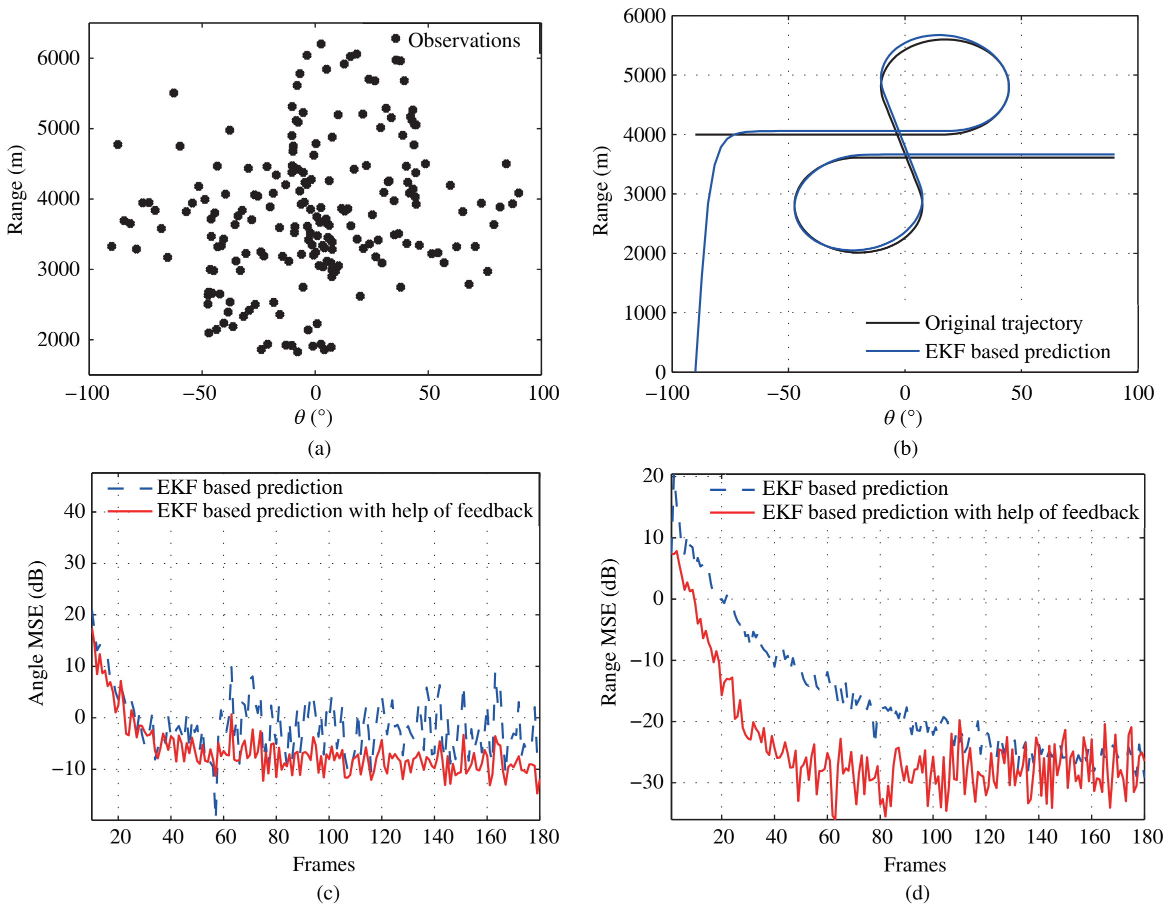

Figure 7 (Color online) Performance analysis of EKF based target position estimation with 180 frames. (a) Observations; (b) EKF based prediction; (c) angle MSE; (d) range MSE.

are forwarded to the EKF based prediction block of receiver to estimate target future direction, i.e., $(\tilde{\theta}_{0,k+1}, \tilde{r}_{0,k+1})$. Instead of taking the target trajectory in Cartesian plane, we convert it to range (r) and theta (θ) axis for making it more relevant to range-angle dependent beamforming of FDA. The target motion is modelled using well-known coordinated turn model. A nonlinear state vector is denoted as $\boldsymbol{x} = [\theta\, \dot{\theta}\, r\, \dot{r}\, \xi]^{\mathrm{T}}$ with θ and $\dot{\theta}$ as target position and velocity component along angle axis, while r and $\dot{r}$ are range and its velocity component along range axis and ξ is turn rate. The nonlinear transitional and measurement matrices are

$$\tilde{\boldsymbol{F}} = \begin{bmatrix} 1 & 0 & 0 & 0 & 0 \\ 0 & \xi & 0 & 0 & 0 \\ 0 & 0 & 1 & 0 & 0 \\ 0 & 0 & 0 & \xi & 0 \\ 0 & 0 & 0 & 0 & 0 \end{bmatrix} \quad \text{and} \quad \tilde{\boldsymbol{H}} = \begin{bmatrix} 1 & 0 & 0 & 0 & 0 \\ 0 & 0 & 1 & 0 & 0 \end{bmatrix}. \tag{63}$$

Figure 7 shows the prediction performance of this EKF based prediction block. The process and measurement noises are taken as zero mean Gaussian with covariance matrices $\boldsymbol{q}$ and $\boldsymbol{R}$, respectively, where $\boldsymbol{q} = \mathrm{diag}[0, \sigma_1^2, 0, \sigma_2^2, \sigma_2^2]$ with $\sigma_1^2 = \sigma_2^2 = 0.25$ and $\boldsymbol{R} = \mathrm{diag}([\sigma_\theta^2, \sigma_r^2])$ with $\sigma_\theta^2 = 0.01$ and $\sigma_r^2 = 0.2$. The SNR is taken as 10 dB. Figure 7(a) shows the observations of the trajectory and Figure 7(b) shows the EKF based target position prediction performance. Figure 7(c) and (d) show the comparison of Extended Kalman filter (EKF) and EKF with feedback loop based prediction performances in terms of measured mean square error with respect to angle and range. This predicted position estimate and estimation error of target position are sent to the transmitter for calculating the non-uniform frequency

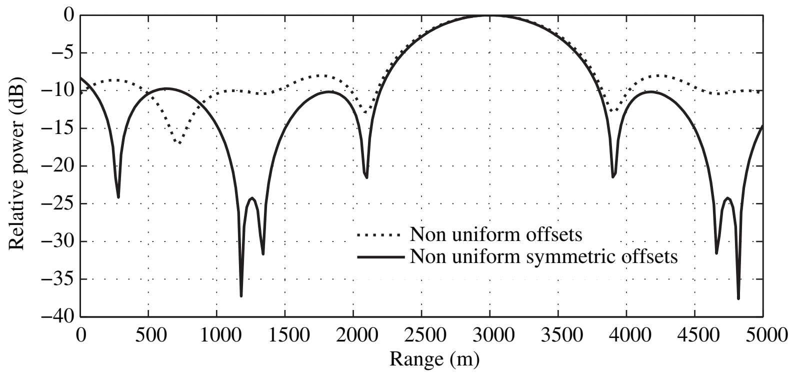

Figure 8 Null depths of FDA with non-uniform non-symmetric and symmetric offsets $N = 11$, $\hat{r}_o = 3$ km, $f_0 = 10$ GHz, $\Delta f = 30$ kHz.

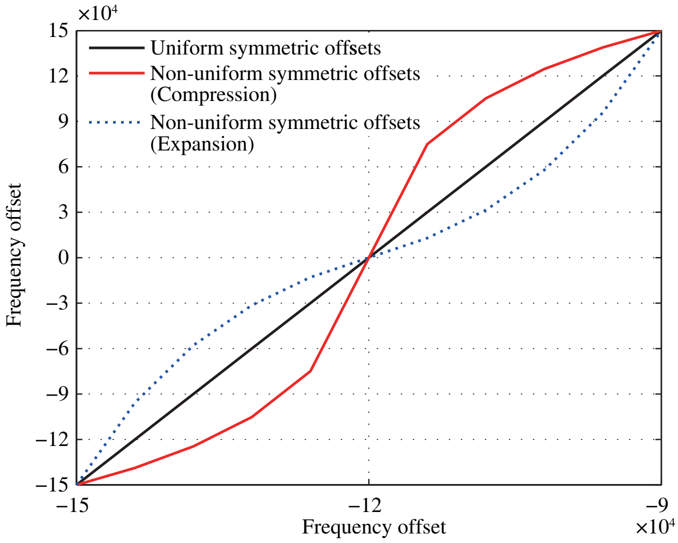

Figure 9 (Color online) Non-uniform frequency offset values of proposed system.

offsets using a suitable companding factor μ.

A basic feed forward neural network (NN) [31] with a multi-layer perceptron (MLP) network having 10 layers has been used for adaptively selecting μ based on $\tilde{\boldsymbol{e}}$. The well-known back propagation algorithm [31] is used for training using predefined estimation error vectors. When $\tilde{\boldsymbol{e}}$ increases the beam pattern is broadened using high value of μ and when $\tilde{\boldsymbol{e}}$ decreases, the beam pattern is sharpened using a small value of μ.

The use of non-uniform symmetric frequency offset may affect the null depth of FDA pattern. Therefore, Figure 8 shows the comparison of the FDA beam pattern for non-uniform and symmetric non-uniform offset coefficients.

It can be seen that by using the symmetric offsets, the disadvantage of losing null depths can be reduced. Therefore, the symmetry around the middle element has been maintained for the subsequent simulations. The transmitter selector, a sub-block of transmitter, decides a suitable value of μ along with mu-law compression or expansion scheme, based on the feedback, i.e., $(\tilde{\theta}_{0,k+1}, \tilde{r}_{0,k+1}, \tilde{\boldsymbol{e}})$. Figure 9 shows uniform and non-uniform frequency offset values for the proposed system. While Figure 10 shows the 3-D and 2-D view of the FDA generated beam patterns using these frequency offset values. Here, we assume that the target estimated position is at $(30°, 3\ \text{km})$. The 2-D view compares these patterns before and after applying companding factors. Figure 10(c) and (d) shows 3-D and 2-D view of the beam using non-uniform frequency offsets calculated by mu-law compression scheme. It results in more directional beam with increased SLL.

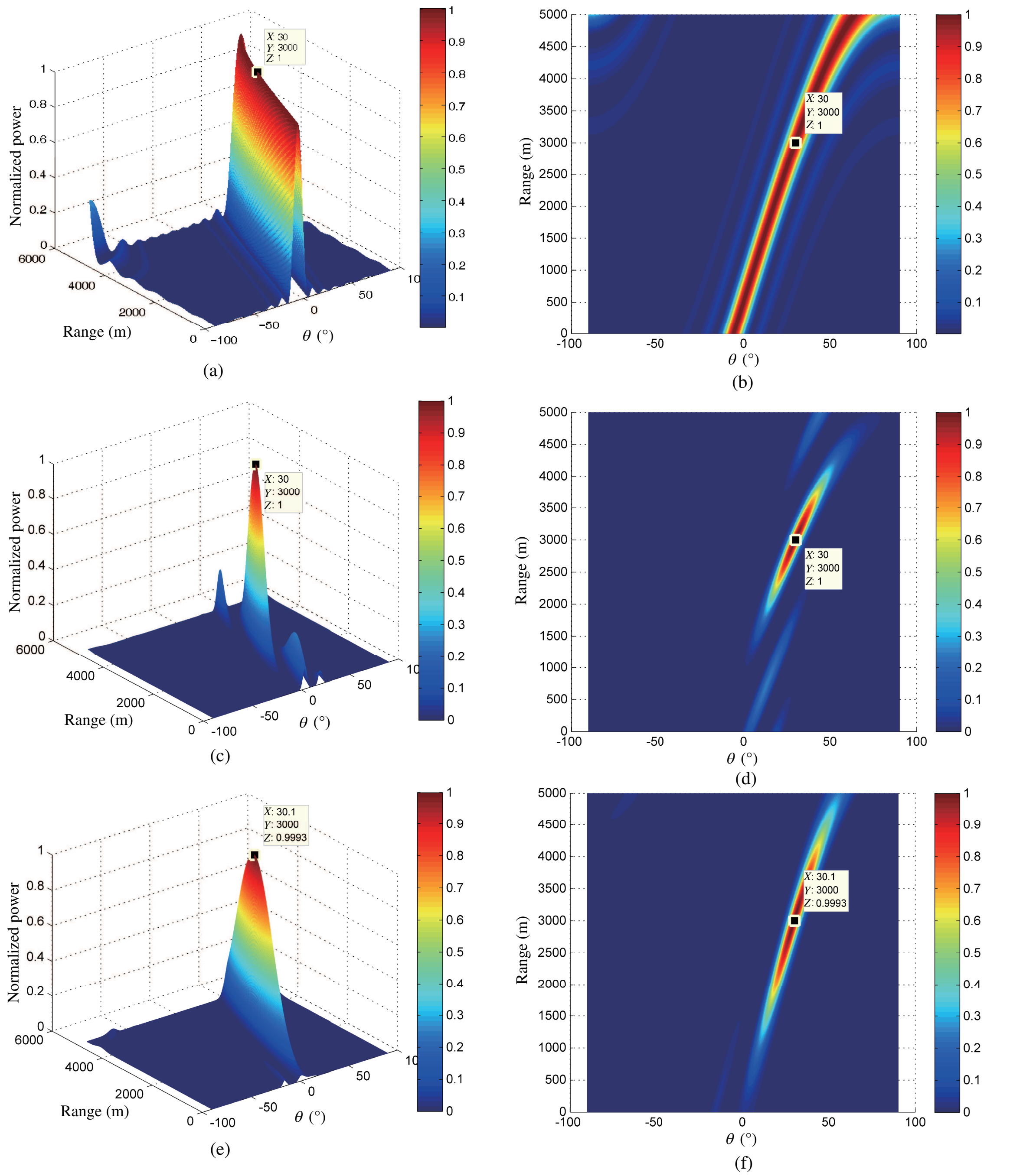

Figure 10 (Color online) 3-D and 2-D views of the FDA generated beam patterns with $N = 11$, $\hat{r}_o = 3$ km, $f_0 = 10$ GHz, $\Delta f = 30$ kHz. (a) and (b) Using uniform symmetric frequency offsets; (c) and (d) using non-uniform symmetric frequency offsets (mu-law compression); (e) and (f) using non-uniform symmetric frequency offsets (mu-law expansion).

On the contrary, using an expanding scheme of mu-law, results in increased HPBW and low SLL (Figure 10(e) and (f)). Lower SLL [24–26] can be achieved by using higher values of μ in expansion scheme. On the top of all, these offsets generate a single maximum, which does not allow the interferers to affect the target- returns, which is reflected in Figure 10(b), (d) and (f), where interferences can be suppressed quite effectively as compared to conventional FDA, which can result in better SINR at receiver. For SINR analysis, an interference is located at $(60^\circ, 4$ km) and the interference plus noise ratio (INR) equals to 30 dB. Figure 11 shows the ouput SINR vs SNR graph for the conventional and proposed FDA design. It can be noticed that the proposed radar has a better SINR performance than that of a conventional FDA

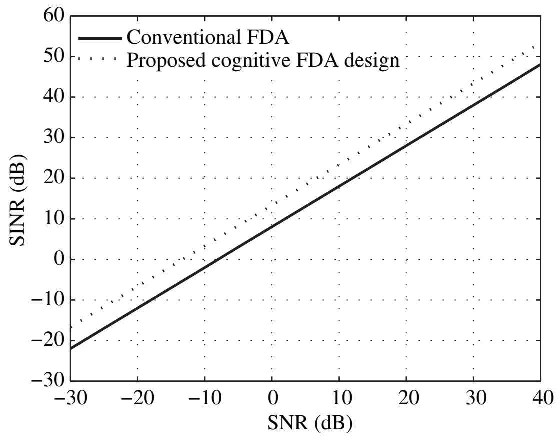

Figure 11 The comparison of output SINR vs SNR of proposed and conventional FDA at fixed INR=30 dB, $N = P = 11$, $\hat{r}_o = 3$ km, $f_0 = 10$ GHz, $D\Delta f = \delta = 30$ kHz.

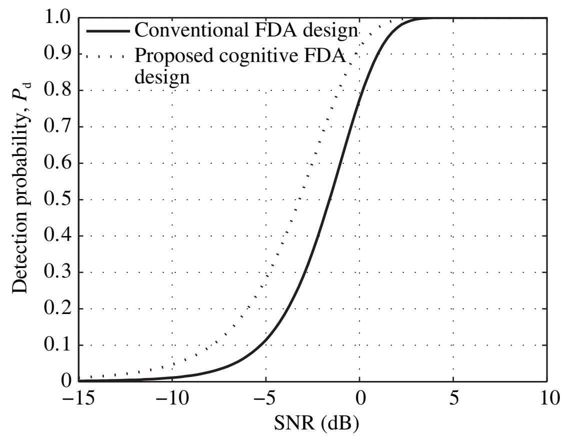

Figure 12 Comparison between the detection performance of proposed FDA and conventional FDA.

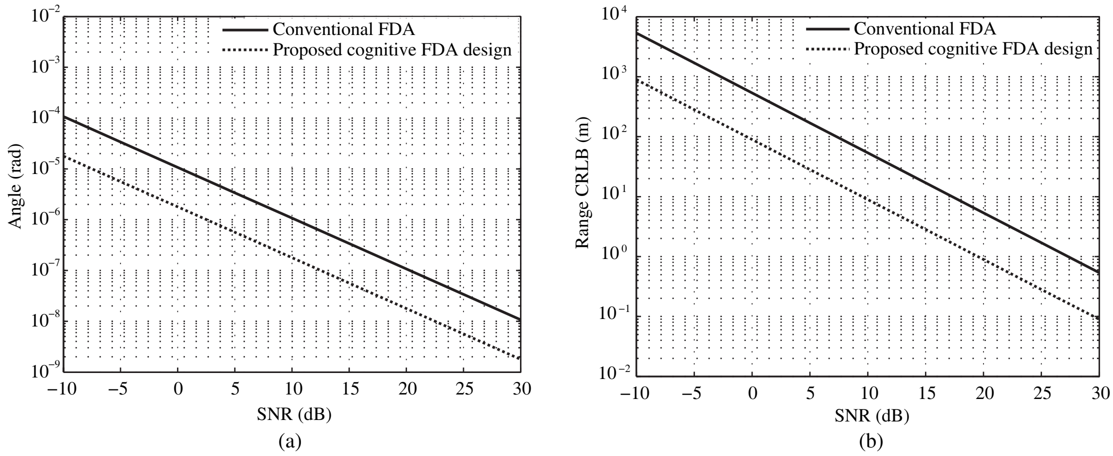

Figure 13 Comparison of CRLB estimation performance vs. SNR. (a) CRLB on target angle; (b) CRLB on target range.

radar. Figure 12 shows the detection performance of proposed FDA design and compares it with conventional FDA radar detection performance with $p_{\mathrm{fa}} = 1\mathrm{e}-4$, which shows a better detection performance of proposed system.

Figure 13(a) and (b) show the comparison of the proposed radar and conventional FDA for CRLB performance on target angle and range, respectively. The proposed approach gives satisfactory estimation performance. In the nutshell, the proposed system learns about the statistical variations of the environment and in response, it makes suitable changes in the design parameter to maintain an improved SINR, detection performance and CRLB.

4 Conclusion

In this paper, the effect of a non-uniform frequency offsets applied along the FDA elements has been analyzed. The well-known mu-law is used to calculate these non-uniform frequency offsets. The cognitive properties, such as feedback, memory and application of adaptive signal processing at the receiver and transmitter have been utilized to maintain an improved performance. Consequently, the proposed radar design achieves an improved SINR that results in better detection performance and improved CRLB for target position estimation as compared to the conventional FDA. Likewise, the symmetrical offsets applied around the middle elements helps in getting improved null depths than that of non-symmetric.

Conflict of interest The authors declare that they have no conflict of interest.

References

1 Antonik P, Wicks M C, Griffiths H D, et al. Frequency diverse array radars. In: Proceedings of IEEE Conference on Radar, Verona, 2006. 215–217
2 Antonik P. An investigation of a frequency diverse array. Dissertation for Ph.D. Degree. Bloomsbury: University College, 2009
3 Huang J J, Tong K F, Baker C J. Frequency diverse array with beam scanning feature. In: Proceedings of IEEE Antennas and Propagation Society International Symposium, San Diego, 2008. 1–4
4 Secmen M, Demir S, Hizal A, et al. Frequency diverse array antenna with periodic time modulated pattern in range and angle. In: Proceedings of IEEE Conference on Radar, Boston, 2007. 427–430
5 Wang W Q. Phased-MIMO radar with frequency diversity for range-dependent beamforming. IEEE Sens J, 2013, 13: 1320–1328
6 Zhuang L, Liu X Z. Precisely beam steering for frequency diverse arrays based on frequency offset selection. In: Proceedings of International Radar Conference "Surveillance for a Safer World", Bordeaux, 2009. 1–4
7 Chen Y G, Li Y T, Wu Y H, et al. Research on the linear frequency diverse array performance. In: Proceedings of IEEE 10th International Conference on Signal Processing, Beijing, 2010. 2324–2327
8 Wang W Q, Shao H, Cai J. Range-angle-dependent beamforming by frequency diverse array antenna. Int J Antenn Propag, 2012, 2012: 760489
9 Shao H, Li J, Chen H, et al. Adaptive frequency offset selection in frequency diverse array radar. IEEE Antenn Wirel Propag Lett, 2014, 13: 1405–1408
10 Khan W, Qureshi I M. Frequency diverse array radar with time-dependent frequency offset. IEEE Antenn Wirel Propag Lett, 2014, 13: 758–761
11 Wang W Q, So H C, Shao H Z. Nonuniform frequency diverse array for range-angle imaging of targets. IEEE Sens J, 2014, 14: 2469–2474
12 Khan W, Qureshi I M, Saeed S. Frequency diverse array radar with logarithmically increasing frequency offset. IEEE Antenn Wirel Propag Lett, 2015, 99: 1–5
13 Sammartino P F, Baker C J, Griffiths H D. Frequency diverse MIMO techniques for radar. IEEE Trans Aerosp Electron Syst, 2013, 49: 201–222
14 Haykin S. Cognitive radar: a way of the future. IEEE Signal Process Mag, 2006. 23: 30–40
15 Xue Y. Cognitive radar: theory and simulations. Dissertation for Ph.D. Degree. Hamilton: McMaster University, 2010
16 Haykin S, Zia A, Xue Y, et al. Control-theoretic approach to tracking radar: first step towards cognition. Digital Signal Process, 2011, 21: 576–585
17 Haykin S, Xue Y, Setoodeh P. Cognitive radar: step toward bridging the gap between neuroscience and engineering. Proc IEEE, 2012, 100: 3102–3130
18 Osman L, Sfar I, Gharsallah A. The application of high-resolution methods for DOA estimation using a linear antenna array. Int J Microw Wirel Tech, 2015, 7: 87–94
19 Grewal M S, Andrews A P. Kalman Filtering: Theory and Practice. Englewood Cliffs: Prentice-Hall, 1993
20 Kaneko H. A unified formulation of segment companding laws and synthesis of codecs and digital compandors. Bell Syst Tech J, 1970, 49: 1555–1588
21 Huang X, Lu J, Zheng J, et al. Reduction of peak-to average power ratio of OFDM signals with companding transform. Electron Lett, 2001, 37: 506–507
22 Huang X, Lu J H, Zheng J L, et al. Companding transform for reduction in peak-to average power ratio of OFDM signals. IEEE Trans Wirel Commun, 2004. 3: 2030–2039
23 Khan S U, Qureshi I M, Zaman F, et al. Null placement and sidelobe suppression in failed array using symmetrical element failure technique and hybrid heuristic computation. Progress Electrom Res B, 2013, 52: 165–184
24 King D, Packard R, Thomas R. Unequally-spaced, broad-band antenna arrays. IRE Trans Antenn Propag, 1960, 8: 380–384
25 Harrington R F. Sidelobe reduction by nonuniform element spacing. IRE Trans Antenn Propag, 1961, 9: 187–192
26 Willey R. Space tapaering of linear and planar arrays. IRE Trans Antenn Propag, 1962, 10: 369–377
27 Basit A, Qureshi I M, Khan W, et al. Hybridization of cognitive radar and phased array radar having low probability of intercept transmit beamforming. Int J Antenn Propag, 2014, 2014: 129172
28 Trees H L V. Optimum Array Processing. New York: Wiley, 2002
29 Wang W Q, Shao H. Range-angle localization of targets by a double-pulse frequency diverse array radar. IEEE J Sele Topics Signal Process, 2014. 8: 106–114
30 Wang Y, Wang W Q, Chen H, et al. Optimal frequency diverse subarray design with Cramér-Rao lower bound minimization. IEEE Antenn Wirel Propag Lett, 2015, 14: 1188–1191
31 Haykin S. Neural Networks and Learning Machines. 3rd ed. Englewood Cliffs: Prentice-Hall, 2009